Radiometric location of partial discharge sources on energised high voltage plant

P. J. Moore, *Senior Member, IEEE,* I. E. Portugues, *Member, IEEE*, and I. A. Glover

Abstract—**Partial discharges (PD) generate wideband radio frequency interference and consequently can be detected using radio receiving equipment. Due to the advances in ultra-high-speed sampling equipment, it is possible to accurately measure the propagation of the PD wavefront as it passes through a 4 element antenna array. From these measurements the 3-dimensional position of the PD source can be calculated using an iterative algorithm. The locating equipment is suitable for use within the vicinity of energised high voltage plant and can locate sources up to 15 m from the array. Results are presented showing the location ability under laboratory and field conditions. The significant advantage of this equipment lies in its ability to detect PD sources in energised plant without the need for outages or electrical connections.**

Index Terms—**partial discharge, digital monitoring, radiometric monitoring, impulsive noise, condition monitoring.**

I. INTRODUCTION

THE use of partial discharge monitoring as a means of non-destructive condition monitoring of power systems plant is widely established. Partial discharges (PD) can be detected by a variety of means including ultrasound, electrical contact methods and radio frequency sensing. These methods can also be applied to the location of PDs which is of considerable interest to utilities since it allows accurate prediction of plant asset life.

A variety of location techniques have been proposed for power transformers including electrical contact methods based on the assumption that the transformer behaves as a linear time-invariant system [1,2]. Using computer modeling, the transfer functions at different locations can be obtained, thus allowing the PD location to be calculated from differences in the waveforms. The use of neural networks to classify the signal distortion inherent in the location of discharges in power transformers has also been investigated [3]. The use of ultrasound sensors on the outside of the tank wall [4] and radiative measurements using UHF couplers [5] have also been explored.

The location of PDs in generators is principally undertaken using two techniques, the delay time and top-top methods [6,7]. The latter assumes the signal diminishes with distance to the origin of the PD. The delay method uses the cross-correlation function between signals to estimate the time of flight of the PD waveform and hence its location; this method is shown to be more accurate than the top-top method [6].

The location of PDs in solid dielectric cable using measurements of traveling electromagnetic phenomena was described over 40 years ago [8]. Subsequently, many studies have improved PD location accuracy and sensitivity [e.g 9-11].

Despite these advances, there has been relatively little progress on a locating system that can be generally applied in a substation environment, rather than specifically applied to an item of plant. In this context the use of radio frequency (rf) remote sensing holds the biggest promise since it can be easily deployed in a substation, does not require any physical contact, and can be applied to any energized plant item.

The development of rf remote sensing techniques for substation use includes field probes [12], and interferometric methods [13,14]. Both of these approaches suffer from the disadvantage of sensing the entirety of the radiated PD waveform. It will be shown later in this paper that only the initial portion of the waveform can be used for location purposes due to the presence of multipath propagation. The location accuracy of these methods will therefore be degraded.

This paper describes a general purpose PD locating system suitable for use in the substation environment. The ability to locate PD relies on the high speed digitization of the antenna signals which has only recently become commercially practicable. The system has been extensively tested on site, and results are presented for several case studies in addition to conventional laboratory studies.

II. IMPULSIVE RADIATION FROM POWER SYSTEM PLANT

The initial rise-time of the current waveform produced by a PD is sufficiently high to cause the frequency spectrum to extend into the radio frequency region. As a consequence, a proportion of the PD energy is radiated into the free-space adjoining the site of the discharge, giving rise to the well known fact that PD can be detected using radiometry.

The majority of radiometric measurements have been made using narrowband, down-converting radio receiving equipment. With recent developments in digital sampling technology, it is now possible to record radiative PD waveforms using a resolution that has not hitherto been possible [15]. These measurements have the following characteristics:

1.   Directly-sampled: the antenna signal is not down-converted before sampling, thus improving the fidelity of the signal.

2. Wideband: typical analogue bandwidths are in the region of 1 GHz, with sampling frequencies in the Giga-Samples per second (GSps) range.

Measurements made using this high-speed digital technology will be referred to as wideband, radiative partial discharge (WRPD) waveforms. Compared to conventional measurements, the extra resolution of WRPD waveforms provides a substantial increase in information content - typically several orders of magnitude. However, the majority of this extra information relates to the substation environment, rather than the nature of the PD. This is explained in the following sections:

A. Nature of Dielectric

The initial rise-time of the current impulse created by a PD electron avalanche differs between dielectrics, being higher for stronger dielectrics, such as oil, than for weaker dielectrics, such as air. Due to the stochastic nature of PDs, it is difficult to model the exact shape of the initial current waveform. Assuming this to be exponential, however, then the resulting spectrum is shown in Figure 1. The effect of stronger and weaker dielectrics can be seen in this figure, with the stronger dielectric being better represented at higher frequencies; this conclusion is supported by experimental evidence [16,17]. This figure also illustrates that the majority of the energy radiated by a PD occurs below 1 GHz. This simple model of PD radiation is in many respects inadequate and under practical conditions the spectra of WRPD waveforms may bear little resemblance to Figure 1. The following sections describe why WRPD waveforms are different when measured within a substation.
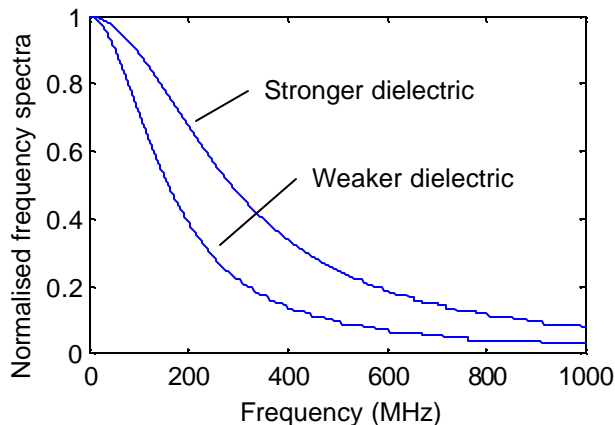

Fig. 1. Frequency spectra for differing dielectrics.

B. Background Noise

WRPD measurements in electrical substations are made in the presence of broadcast transmissions. Figure 2 shows the spectrum of background noise in a typical substation. The levels of broadcast transmissions vary considerably, generally being higher for substations close to metropolitan areas. Additionally, the presence of several PD sources can also make the noise environment appear to be cluttered. For the locator described in the following sections this is not a problem since multiple sources can be distinguished geometrically. Due to the short duration of a WRPD impulse

(<1 µs), the probability of 2 impulses from differing sources appearing coincidently is extremely small. Thus, the major source of background noise is therefore broadcast transmissions.

C. Nature of radiating structure

The conducting metalwork attached to the PD source – typically busbars and connecting links - influences the radiation of rf energy. Due to resonance, the specific shapes and configurations of these conductors leads to preferential radiation of certain frequencies, whilst reducing that of others. This effect leads to the distortion of the ideal PD spectrum described in section A.
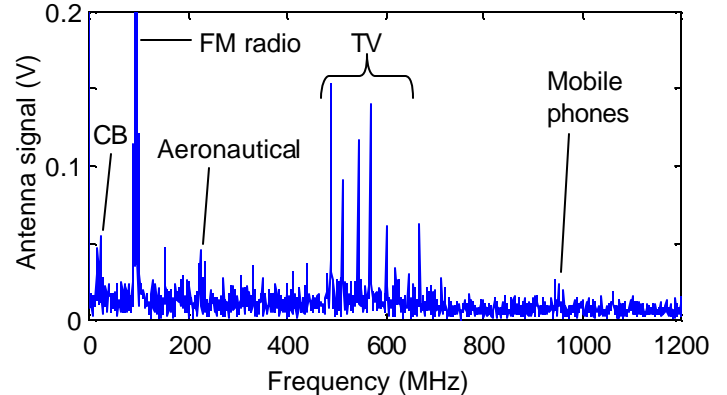

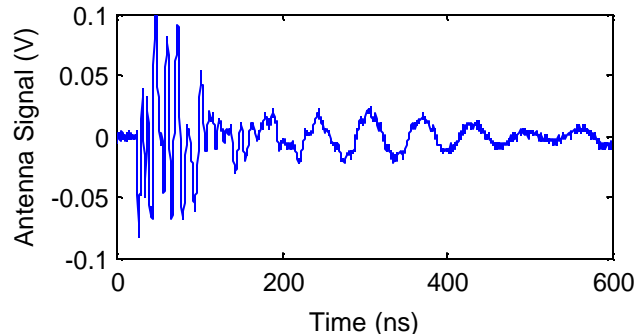Fig. 2. Background radio spectrum recorded by locating equipment..

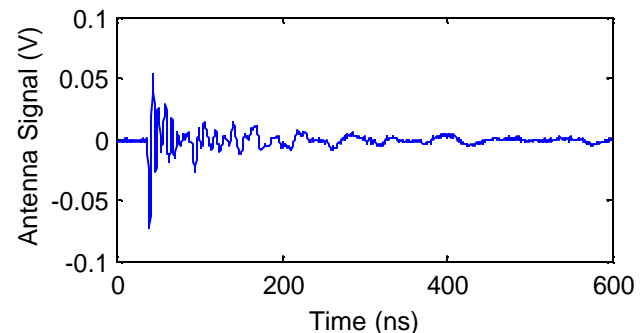Fig. 3. Line defect WRPD waveform recorded with antenna 1.

Fig. 4. The same WRPD as Fig. 3 recorded from adjacent antenna (2). Antennas 1 and 2 were approximately 2 m apart; the signals were recorded synchronously from each antenna.

D. Nature of Substation Environment

In addition to the effect of the radiating structure described in C, other metallic structures in the vicinity of the source and the receiving antenna will influence the nature of the WRPD

signal due to scattering and reflection. Reflections cause multi-path propagation of the WRPD impulse and result in the signal measured at the antenna being the sum of the direct path signal between the PD source and the antenna, and multiple reflected signals. Due to the large number of reflecting surfaces within the substation environment, the combined effect of C and D causes the detailed nature of the WRPD waveform to be influenced more by the local environment and the position of measurement, than by the inherent properties of the dielectric causing the PD. This is illustrated in Figures 3 and 4 which show PD signals caused by a defective overhead line conductor measured simultaneously from two different positions spaced 2 m apart. The discharge source was approximately 20 m distant from each antenna. It is apparent that the waveforms are remarkably dissimilar, given the small change in antenna position.
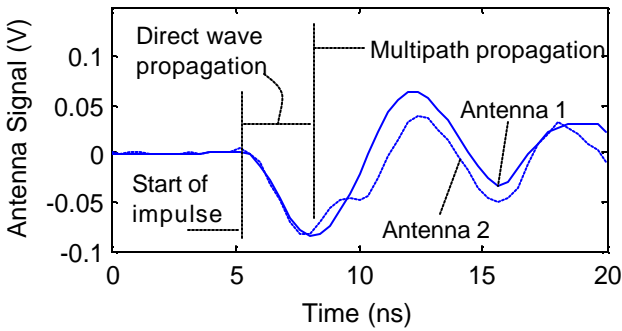

Fig. 5.   Impulse wavefronts from Figs 3 and 4. Arbitrary timescale, waveforms corrected for distance to source.

III.   LOCATION OF PD IMPULSES

The previous section asserts that the propagation environment, rather than the PD, has the greatest impact on WRPD waveforms. Despite this, the physical location of the discharge source can be found by analysing the initial part of the WRPD wavefront that represents the direct path of signal from the source before any reflections occur. The distinction between the direct path and multiple reflected path components can be seen in Figure 5 which shows the initial wavefronts of the signals of Figures 3 and 4. In this figure the signals have been corrected for the time delay and amplitude differences caused by unequal path lengths. It can be seen that the initial 3 ns of the signals are the same at both antennas; this is the *direct wave*. Following the direct wave, the effect of reflection leads to differences in the received signals; this is the multi-path region. The time between the direct wave and the first reflection is variable, being a function of the positions of reflecting objects in the vicinity of the source and antennas.

The 3-dimensional location of the discharge source can be determined using a passive 4-antenna array with direct sampling capable of measuring the arrival time of the direct wave to sub-ns accuracy. A conceptual view of the process is shown in Figure 6. Four antennas at known 3-dimensional positions are situated close to the discharge source. The times of flight of the direct wave from the source to the antennas are shown as t_1, t_2, t_3 and t_4. By measuring the time differences as the direct wave propagates through the antenna array, e.g. $t_{12} = t_1 - t_2$, the source position can be calculated. The calculations to perform this are described in following sections.
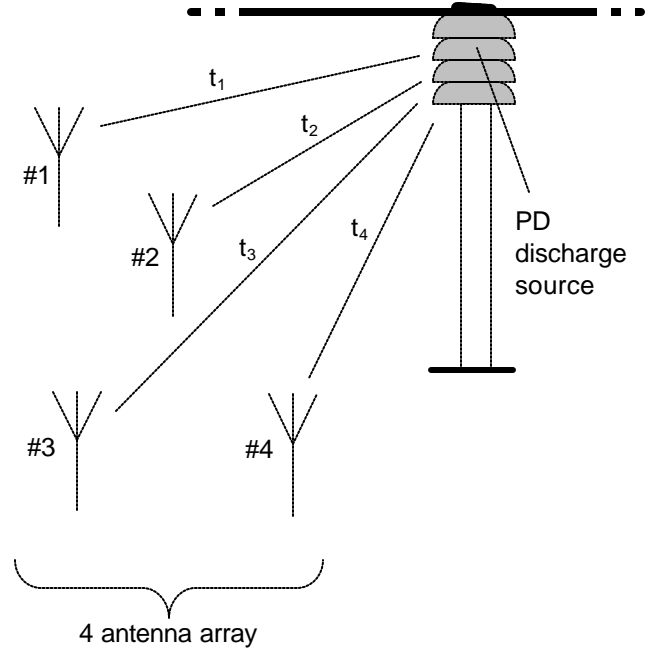

Fig. 6.   Conceptual view of PD discharge location process.

A. Arrival Time Difference Calculation

The arrival time difference calculation is achieved in two steps:

1.   The direct wave arrival time at the array is found approximately using a simple thresholding technique on the digital record of each antenna signal. This gives an answer to within one or two samples.

2.   From a knowledge of the approximate position of the direct wave in each channel, the arrival time differences are more accurately evaluated using a cross-correlation technique.

The antenna signals are simultaneously sampled to give a digital sequence for each channel: $x_q(k)$, where q =1,2,3 or 4, and $1 \leq k \leq N$. In practice, a value of N = 5000 has been used which corresponds to a sequence length of 2 µs at a sampling frequency of 2.5 GSps.

1) Thresholding

Thresholding finds the approximate position of the direct wave by comparing the digital sequence for each channel against a threshold: the position of the direct wave is identified where the sequence value exceeds the threshold. It is assumed that the first *m* samples of each sequence will not contain the WRPD impulse waveform, and hence can be used to characterise the background noise. Thus, the peak background noise value, $\hat{s}_q$, is found from:

Eqn 1

$$\hat{s}_q = \max |x_q(n)| \qquad for\ n = 1, m$$

The threshold value, T_q, is set to a multiple of $\hat{s}_q$ – in practice a multiple of 2 has given satisfactory results. The position of the direct wave, d_q, is found as the first value of n that satisfies $|x_q(n)| > T_q$ as n is varied from m to N. Note that absolute values of the signal and threshold are used to avoid problems of polarity, since the initial direction of the impulse is dependent on the voltage polarity. Although crude, the threshold technique has the advantage of being insensitive to the multi-path region, acting only on the direct wave. The arrival time difference is found by subtracting the values between antennas, e.g. $d_{12} = d_1 - d_2$.

2) Cross-Correlation

The arrival time difference is improved by cross-correlating the direct wave region of the signals from the two antennas. Cross-correlation finds the similarity of the two signals and, with the use of interpolation, allows resolution of the time-delay to fractions of a sampling interval. Analysis based on the direct-wave region of the impulse is ensured by windowing the signal around the impulse position found from the previous thresholding approximation. Assuming the signal is windowed p samples either side of the position identified by thresholding, the windowed value for each channel $y_q(n)$ can be expressed as:

$$y_q(n) = x_q(d_q - (p+1) + n) \qquad for\ n = 1, 2p+1 \qquad \text{Eqn 2}$$

The extent of this window must be critically chosen to ensure that it does not extend into the multipath region: typically $p = 5$ samples. Cross-correlation of the windowed signals is achieved as follows:

$$R_{12}(j) = \sum_{n=0}^{2p-j} y_1(n+j) y_2(n) \qquad for\ j = -p, p \qquad \text{Eqn 3}$$

where R_{12} is the cross correlation product for channels 1 and 2. An example is shown in Figure 7; the delay between the windowed signals, $?_{12}$, is found from the offset of the peak of the cross-correlation product from the origin. From the inset in Figure 7, which shows the peak in greater detail, this delay can be seen to be +0.8 ns (note that the calculation is performed in terms of sample intervals, rather than time). The accuracy of this result can be improved by interpolating the cross-correlation product sequence to a higher sampling rate since, it is clear from Figure 7, that the true peak lies between 2 samples. Although the true peak may be found to very high accuracy by high interpolation factors (i.e. ratio of post to pre-interpolated data), experience of this approach suggests that interpolation to greater than 10 times the original sampling frequency does not lead to any greater resolution of the time delay due to the presence of broadcast noise. Further, in the presence of PD signal-to-noise voltage ratios (described later) of less than 10, it is unlikely that interpolation will improve the arrival time difference accuracy. Application of a 10×, lowpass interpolation algorithm to the data of Figure 7 improves the resolution of the delay to +0.68 ns, compared to +0.8 ns
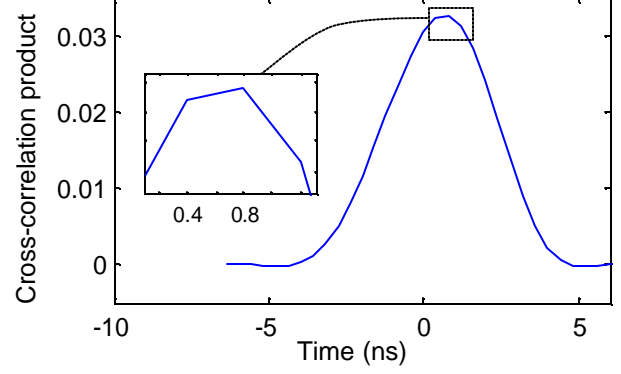
without interpolation.

Fig. 7. Cross-correlation of wavefronts from figs 3 and 4. Inset shows detail around peak.

The total arrival time difference is found from the sum of the thresholded arrival time difference and the cross-correlation delay, e.g.

$$t_{12} = d_{12} + \Delta_{12} \qquad \text{Eqn 4}$$

This procedure is normally conducted by taking one channel - usually channel 1 - as a reference, to yield t_{12}, t_{13} and t_{14}. These values are required for the location algorithm which is described in the next section. However, it is also possible to find all additional time delays between the 4 channels, i.e. t_{23}, t_{34} and t_{42}, which are needed under certain conditions described later.

B. Location Algorithm

Location of the PD source involves simultaneous solution of a set of non-linear geometric equations. Let a 3-dimensional position be represented in rectangular coordinates as (x,y,z), with a subscript 's' denoting the PD source, and subscripts 1 to 4 (or more generally q) denoting the antenna positions. The PD impulse is assumed to be launched from the source position at unknown time τ, and to arrive at the four antennas at times t_1 to t_4. Assuming that the WRPD wavefront expands spherically from the source position at the velocity of light, c, the propagation can be described by the following generic equation:

$$c^2(t_q - t)^2 = (x_s - x_q)^2 + (y_s - y_q)^2 + (z_s - z_q)^2 \qquad \text{Eqn 5}$$

Since τ is unknown, and the arrival times are only known as differences, the propagation equations can be more usefully written as:

$$ct_{12} = g_1 - g_2 \qquad \text{Eqns 6}$$
$$ct_{13} = g_1 - g_3 \qquad \text{Eqns 7}$$
$$ct_{14} = g_1 - g_4 \qquad \text{Eqns 8}$$

where $g_q = \sqrt{(x_s - x_q)^2 + (y_s - y_q)^2 + (z_s - z_q)^2} \qquad \text{Eqn 9}$

and $t_{12} = t_1 - t_2$, etc. Equations 6-8 contain three unknowns (x_s, y_s, z_s) and can be solved by iteration; Appendix I describes a Newton-Raphson solution approach that has worked

satisfactorily. Execution of this algorithm can result in three possible outcomes:

1. The algorithm converges on the source location.
2. The algorithm cannot converge, but enters into a limit cycle where the positions of subsequent iterations lie on a line passing through the antenna array and the source.
3. The algorithm diverges asymptotically.

Outcomes 1 and 2 correspond to the PD source being located close to or far from the antenna array as described in the next section. Outcome 3 is a function of the ratio of WRPD signal to background noise. In the presence of noise, the time of arrival of the WRPD signal can be distorted. Since background noise varies spatially, it is possible for a set of arrival times to be calculated that do not correspond to a physical source position: in this case the algorithm can fail to converge. This is a particular problem where the antenna spacing is small. It is possible to recover this situation by making small adjustments to the time delays to find the nearest position of convergence. A technique for this - the noisy signal algorithm - is described in Appendix II.

C. Location Accuracy

The location accuracy depends on the configuration of the 4-antenna array and the distance to the source. In general the accuracy is difficult to quantify due to the non-linear nature of the location equations and the arbitrary array configuration afforded by site conditions. Figure 8 gives an appreciation of the accuracy that can be expected for a square array of side length 3 m. In this plan view the antennas are shown as circles close to the origin and the remaining points represent source locations in 3-dimensional space (up to 3 m vertically) where the time delays on the antennas correspond to exact integer multiples of the sampling interval (0.4 ns, $f_s = 2.5$ GSps). Source locations not coinciding with the points shown in Figure 8 will be located to the nearest point. It can be seen, therefore, that sources within 5 m of the array will be located to a high accuracy – typically a few tens of cm – whereas sources at 12 m can suffer a location error in excess of 2 m. The maximum range of the array occurs along the array diagonal, and the maximum resolution occurs parallel to the array side. Source locations originating beyond the limits of the points shown in Figure 8 will not be located, but the 3-D bearing to the source can be found with high precision, typically to within 1°. Figure 9 shows the location ability of a Y-shaped array, where the larger antenna spacing is 2 m. This configuration is seen to be inferior to the square array in terms of location accuracy, although the antenna spacing is slightly smaller.

Note that these figures are conservative estimates of the locating accuracy since they do not take into account the interpolation of the cross-correlation product that allows time delays to be estimated to fractions of a sampling interval.
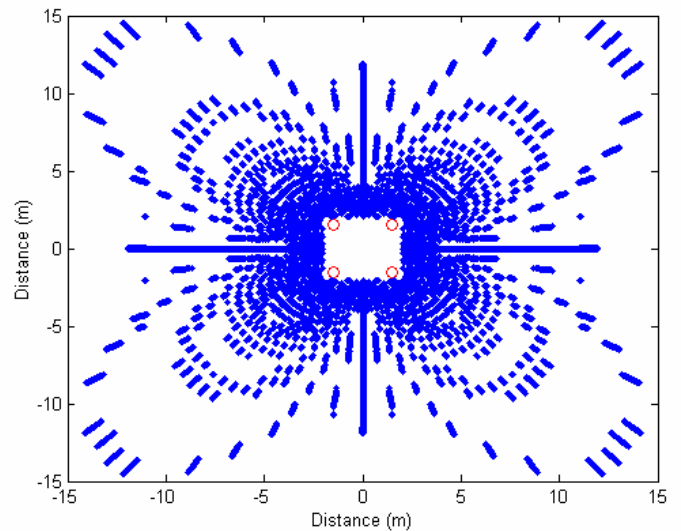

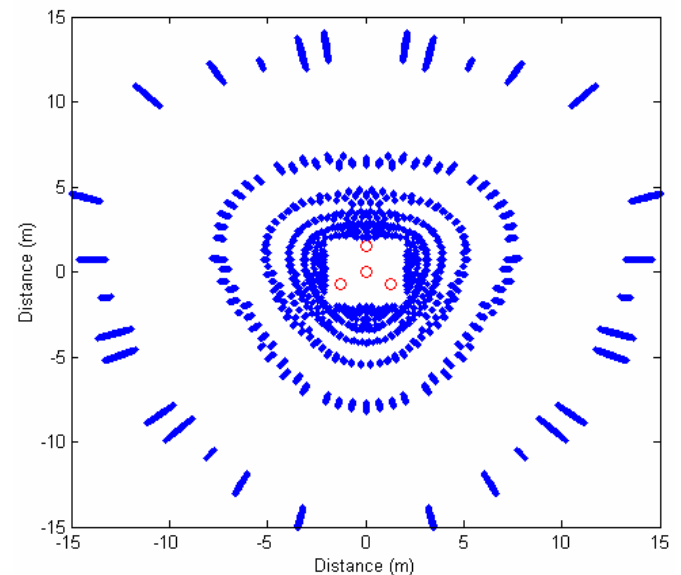Fig. 8. Location performance of square array with antenna spacing 3 m.

Fig. 9. Location performance of Y-shaped array with antenna spacing 2 m.

IV. RECORDING HARDWARE

The recording equipment consists of diskcone antennas, sampling scope and personal computer. The diskcone antenna, Figure 10, consists of a dual cone element and an earth plane, and is both broadband and omnidirectional. This design has been extensively used for locating impulsive noise and provides a relatively flat frequency response to the vertical electric field in the range 0.1-1 GHz, with a constant impedance of 50 Ω.

The antenna signals are digitized with a Tektronix TDS 7104 Digital Phosphor Scope that can sample four channels synchronously at a sampling rate of 2.5 Giga samples per second (GSps) and has an analogue bandwidth of 1 GHz. An important feature of this scope, given the repetitive nature of PD, is the segmented memory architecture that allows the main sampling memory of 2 M-samples per channel to be segmented

into separately triggered buffers of 5000 samples each. Each time a buffer is triggered, the scope records the start time as a timestamp with a resolution of 10^{-9} s. The 4-channel memory data and accompanying timestamps are downloaded to a personal computer (PC) via a GPIB connection. Conventional amplitude triggering of the scope is used.
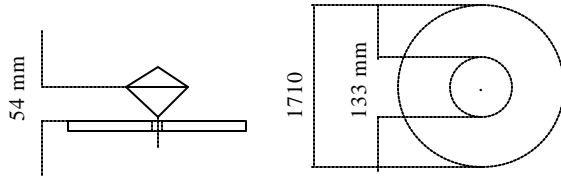

Fig. 10. Diskcone antenna. The cone section was machined from solid aluminium. The base plate was fabricated from 2 mm thick aluminium sheet.

V. SITE APPLICATION

a) Setting-up

The equipment is deployed on site in the vicinity of suspect equipment, or in positions where significant radio frequency interference (RFI) has been observed, e.g. with the use of a RFI meter. The four antennas are situated close to the ground. Due to the limitations of substation space, and the need to situate the antennas away from metalwork to avoid reflections, it is rarely possible to form an exact square and so a quadrilateral form is used. The antennas are connected to the scope using highly screened coaxial leads. It is necessary to ensure that the propagation delays of all four leads are identical, otherwise the PD source location will be in error. This is achieved by constructing the leads with equal lengths of coaxial cable and subsequently checking their impulse propagation delays using a network analyzer. Lead lengths of 50 m have been successfully used on site, but, with a high-quality, highly screened coaxial cable, lengths of up to several hundreds of metres should be possible.

b) Mapping considerations

Following siting of the antennas, their positions are measured to the nearest cm (using a measuring tape), in relation to a convenient datum – e.g. relative to some nearby equipment. From these measurements, the 3-dimensional rectangular coordinates of the antennas are calculated for inclusion in the solution of location equations 6-8. Inherent in this process is the establishment of an origin and 'x' and 'y' directions. It is sometimes possible to use existing substation mapping data to help in relating the PD source location to the substation equipment.

c) Measurements

All data is recorded on site and analysed for PD location off-line. The trigger level and sensitivity of the oscilloscope are set according to site conditions. In general, WRPD waveforms do not exceed 100 mV in amplitude. Data suitable for identifying the location of a continuous PD source can be recorded within a few minutes. In view of the fact that many PDs are intermittent, however, it is possible (with suitable weatherproofing) to leave the equipment for longer-term measurements, e.g. monitoring periods of days or weeks.

VI. RESULTS

The locator has been extensively tested in a variety of site trials. This section describes the results of a laboratory test and two site case studies.

A. Laboratory Test

Locating accuracy was tested under laboratory conditions. Figure 11 shows a plan view of the arrangement consisting of a single phase test transformer, PD cell containing a point-plane gap with varying dielectrics, capacitive divider, connecting busbars and the locator 4-antenna array arranged in a Y configuration. The transformer voltage was raised until PD inception (40 – 60 kV depending on the dielectric). The PD cell and busbars were located at a height of 1.2 m.
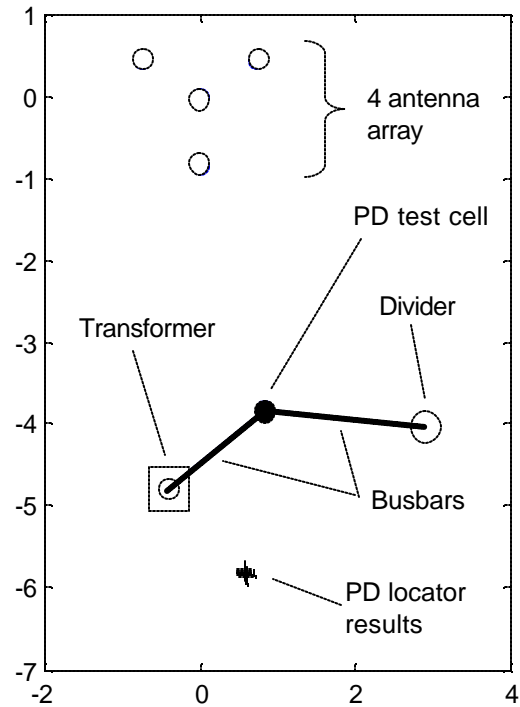

Fig. 11. Laboratory test arrangement (axes in metres).

The arrival time differences from the locator were calculated as described in the previous section. When applied to the location algorithm, divergent behaviour was observed and so the 'noisy' signal algorithm described in Appendix II was applied. Three dielectrics were used in these tests: air, oil and SF_6. From the locator results shown in Figure 11, it can be seen that there is little difference in the locations amongst these dielectrics. Typical location results are shown in Table 1 together with PD signal-to-noise voltage ratio (SNVR). The PD SNVR is a useful metric for describing the size of the PD in relation to the background noise, it is defined as the ratio of the direct wave peak voltage to pre-impulse noise peak voltage. It can be seen from table 1 that the inception level PD of differing dielectrics yields varying SNVR values, although this did not affect the location. The error in the location (< 2 m) is related to several factors. Firstly the low PD signal to noise ratio would not allow interpolation of the cross-correlation

product to improve the arrival time difference accuracy. Secondly, given this fact, it can be seen by reference to Figure 9 that the PD source is at the extremities of the useful Y-array area.

Dielectric	X (m)	Y (m)	Z (m)	PD SNR
Air	0.589	-5.826	1.556	5.5
Oil	0.591	-5.835	1.559	6.5
SF$_6$	0.585	-5.782	1.570	3.7

Table 1: Typical location results for laboratory tests.

B. Case Study 1: Capacitor Bank Investigatiot.

This result was recorded at a 132 kV substation following observations of increased levels of RFI when a capacitor bank was energised. The location result is shown in Figure 12, which is superimposed on a site plan. The vertical height of the locations are in the region of 3.5 m, which corresponds the top row of capacitors. The PD SNR for these results was approximately 25. Presence of the PD was confirmed using a directional ultrasound gun. This situation is being monitored by the utility.
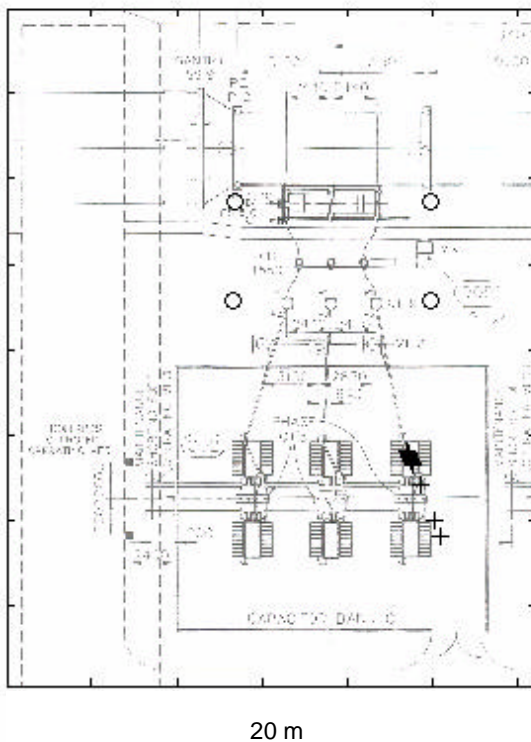

Fig. 12. Capacitor bank investigation. Antennas and PD locations shown superimposed on site plan.

C. Case Study 2: Overhead line defect

This study was conducted as the result of a complaint brought by residents whose house is situated underneath a distribution company 132 kV double circuit overhead line. The complaint concerned distortion of television and FM radio reception which was observed to increase during dry conditions. The antenna array was set up in the garden of the complainants. The measured PD SNR was 15. Figure 13 shows

three orthographic views of the antennas, overhead line, houses and locator output.
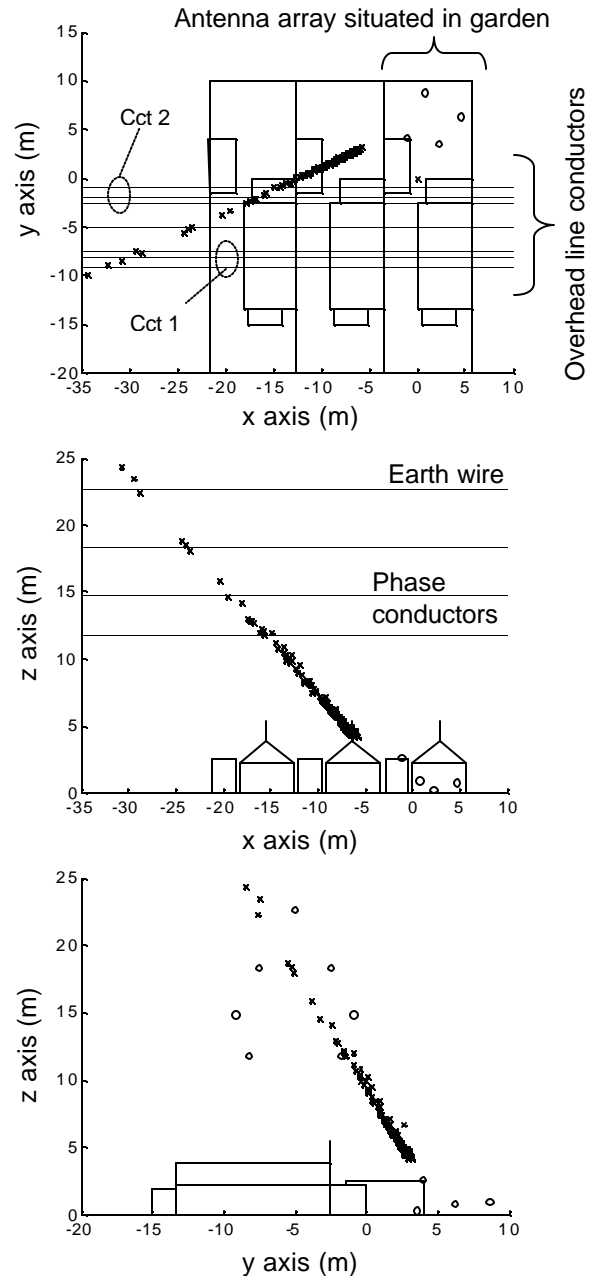

Fig. 13. Overhead line investigation. Three orthographic views showing the PD bearing from the locator in relation to buildings and the overhead line.

Application of the conventional locator algorithm revealed that the PD source was too far removed from the array (in excess of 20 m) for convergence on an exact location. In this situation the algorithm will iterate continuously, each iteration producing a location output that lies on the line joining the array centre and the source. By showing the results of over 300 separately recorded WRPD impulses, and halting the algorithm after 25 iterations, this line can be clearly seen. (Note that algorithm results occurring close to the array have been suppressed.) In this case study, the lack of a definitive location

is not a disadvantage since the location of the PD source is clearly identified, being the lowest phase on circuit 2, situated approximately 15 m horizontally to the left of the complainants' house. Observation of the region of the line identified by the locator through binoculars showed damage to the outer conductor strands.

VII. CONCLUSIONS

A radiometric partial discharge locator has been developed that is suitable for application in the vicinity of energized high-voltage plant. The locator is based on ultra-high-speed, directly-sampled antenna measurements that allow the direct wave component of the radiated signal to be resolved. The results of the locator show that it can locate PD sources to within a few metres if the distance to the antenna array is less than 15 m. PD sources situated at greater than this distance cannot be located, but can be identified through the 3-dimensional bearing of the source from the antenna array.

The significant advantages of this equipment are:
1. No electrical connections are made to the plant,
2. No plant outage is required,
3. Measurements are made whilst the plant is energized,
4. The equipment is portable and easily site-deployable,
5. The equipment can be left to monitor unattended in situations where the PD source is intermittent.

VIII. FURTHER WORK

Further development of the locator is currently being pursued:
1. Vehicle based solution: to improve the application of the locator a version is currently being fitted to a van. This version has a fixed array mounted to the roof, with the sampling equipment being located within, and powered from, the van.
2. Substation monitoring: a system installed in a substation with a fixed array on the roof of the substation building is currently under trial.

Both of these projects are in progress and is hoped to report on developments in due course. Additionally, the following investigations are being planned:
3. Understanding of the emission of radiative PD signals: more research is required to explain this effect, particularly where the PD source is located within a steel tank, such as defects in transformers.
4. Correlation between PD magnitude (pC) and radiated field measurements.

IX. ACKNOWLEDGEMENTS

X. APPENDIX I: SOLUTION OF LOCATION EQUATIONS

Equations 6 – 8 can be solved by application of the Newton Raphson technique. Estimates of the variables x_s, y_s, and z_s will be denoted as x_s', y_s', and z_s' respectively. To correct the estimates, a corrective term must be added to give the correct solution, e.g. $x_s' + \Delta x_s = x_s$ and similarly for the other variables where Δx_s, Δy_s, and Δz_s are the corrective terms. Equations 6 – 8 can be re-expressed as:

$$f_{12} = g_1 - g_2 - ct_{12} \qquad \text{Eqn A1}$$

etc, where functions f_{12}, f_{13} and f_{14} will be zero as stated, but generally non-zero if estimated values are used, i.e. x_s replaced with x_s', etc. These functions can be expressed in a matrix formulation:

$$F(x_s, y_s, z_s) = [f_{12} \; f_{13} \; f_{14}]^T \qquad \text{Eqn A2}$$

Substituting equation A2 with the estimated variables and

$$F(x_s, y_s, z_s) = F(x_s', y_s', z_s') + \Delta' \frac{dF(x_s', y_s', z_s')}{d(x_s, y_s, z_s)} \qquad \text{Eqn A3}$$

expanding with the first two terms of a Taylor series yields:
where $\Delta' = [\Delta x_s' \; \Delta y_s' \; \Delta z_s']^T$ is a matrix of corrective terms. The final derivative term in equation A3 is a 4×4 Jacobean matrix of partial derivatives, J. This matrix is specifically evaluated as:

$$J = \begin{bmatrix} \dfrac{x_s' - x_1}{g_1} - \dfrac{x_s' - x_2}{g_2} & \dfrac{y_s' - y_1}{g_1} - \dfrac{y_s' - y_2}{g_2} & \dfrac{z_s' - z_1}{g_1} - \dfrac{z_s' - z_2}{g_2} \\ \dfrac{x_s' - x_1}{g_1} - \dfrac{x_s' - x_3}{g_3} & \dfrac{y_s' - y_1}{g_1} - \dfrac{y_s' - y_3}{g_3} & \dfrac{z_s' - z_1}{g_1} - \dfrac{z_s' - z_3}{g_3} \\ \dfrac{x_s' - x_1}{g_1} - \dfrac{x_s' - x_4}{g_4} & \dfrac{y_s' - y_1}{g_1} - \dfrac{y_s' - y_4}{g_4} & \dfrac{z_s' - z_1}{g_1} - \dfrac{z_s' - z_4}{g_4} \end{bmatrix}$$

$$\text{Eqn A4}$$

Finally, the corrective terms of the estimated variables can be evaluated from:

$$\Delta' = J^{-1} F(x_s', y_s', z_s') \qquad \text{Eqn A5}$$

from which improved estimates of the unknown variables may be found. Application of this procedure will find the 3-dimensional PD source position to an accuracy of 0.15 m in, typically, 10 iterations. Initially, the unknown variables are set to zero.

XI. APPENDIX II: SOLUTION FOR NOISY SIGNALS

In the presence of high levels of background noise, the error in the time delays can lead to divergent behaviour of the location algorithm. This can be overcome by the following procedure:
1. The time delays t_{12}, t_{13} and t_{14} are calculated as previously described, but additionally t_{23}, t_{34} and t_{42} are

also evaluated – note that these latter time delays are not used in the location solution.

2. A small adjustment is made to the time delays: $t_{12}+?_{12}$, $t_{13}+?_{13}$ and $t_{14}+?_{14}$.

3. An error function, e, is calculated describing the difference between the adjusted time delays and the additional time delays unused in the solution:

$$e = \sqrt{h_{23}^2 + h_{34}^2 + h_{42}^2} \qquad \text{where}$$

$h_{23} = (t_{12} + \Delta_{12} - (t_{12} + \Delta_{12}) - t_{23})$ etc. Eqn A6

4. The solution algorithm is applied using the adjusted time delays.

5. The above procedure is repeated for all combinations of time delay adjustments $?_{12}$, $?_{13}$ and $?_{14}$ in the range -0.5 to +0.5 sampling intervals at steps of 0.1.

6. The PD source position is found from the converged algorithm solution that minimizes e.

XII. REFERENCES

[1] Z. D. Wang, P. A. Crossley, and K. J. Cornick, "Partial discharge location in power transformers using the spectra of the terminal current signals", *Eleventh International Symposium on High Voltage Engineering (IEE Conf. Publ. No. 467)*, 1999, vol. 5, pp. 58 -61.

[2] P. Werle, H. Borsi, and E. Gockenbach, "A new method for partial discharge location on power transformers based on a system theoretical approach", *6th International Conference on Properties and Applications of Dielectric Materials*, 2000, vol. 2, pp. 831 – 834.

[3] P. Werle, A. Akbari, H. Borsi, and E. Gockenbach, "Partial discharge localisation on power transformers using neural networks combined with sectional winding transfer functions as knowledge base", *International Symposium on Electrical Insulating Materials*, 2001, pp. 579 –582.

[4] K. Raja and T. Floribert, "Comparative investigations on UHF and acoustic PD detection sensitivity in transformers", *IEEE International Symposium on Electrical Insulation*, 2002, pp. 150-153.

[5] M. D. Judd, G. F. Cleary and C. J. Bennoch, "Applying UHF partial discharge detection to power transformers", *IEEE Power Engineering Review*, August 2003, pp 57 – 59.

[6] H. J. van Breen, E. Gulski and J. J. Smit, "Localizing the Source of Partial Discharges in Large Generators", *6th International Conference on Properties and Applications of Dielectric Materials*, 2000, vol. 2, pp 868-871.

[7] Y. Tian, P. L. Lewin, A. E. Davies, S. J. Sutton and S. G. Swingler, "Partial discharge detection in cables using VHF capacitive couplers", *IEEE Transactions on Dielectrics and Electrical Insulation*, vol. 10, issue 2, April 2003, pp. 343-353.

[8] F. H. Kreuger, "Discharge detection in high voltage equipment", Temple Press, London, 1964.

[9] J. P. Steiner, P. H. Reynolds and W. L. Weeks, "Estimating the Location of Partial Discharges in Cables", *IEEE Transactions on Electrical Insulation*, vol. 27, no.1, February 1992.

[10] B. Quak, E. Gulski, F. J. Wester and P. N. Seitz, "Advanced PD site location in distribution power cables", *Seventh International Conference on Properties and Applications of Dielectric Materials*, Vol. 1, 2003, pp. 183-186.

[11] M. S. Mashikian, "Preventive maintenance testing of shielded power cable systems", *IEEE Transactions on Industry Applications*, Vol. 38, Issue 3, May/Jun 2002, pp 736 -743.

[12] E. Lemke, "A new procedure for partial discharge measurements on the basis of an electromagnetical sensor", *Fifth International Symposium on High Voltage Engineering*, 1988, Paper 41.02.

[13] A. Tungkanawanich, Z. I. Kawasaki, J. Abe and K. Matsuura, "Location of partial discharge source on distribution line by measuring emitted pulse-train electromagnetic waves", *IEEE Power Engineering Society Winter Meeting*, 2000, Vol. 4 , pp. 2453-2458.

[14] M. Kawada, "Ultra Wide Band VHF/UHF Radio Interferometer System for Detecting Partial Discharge Source", *IEEE Power Engineering Society Winter Meeting*, 2002, Vol. 2 , pp. 1482 – 1487.

[15] A. Cavallini *et al*, "A new approach to the diagnosis of solid insulation systems based on PD signal inference", *IEEE Electrical Insulation Magazine*, March/April 2003, Vol. 19, No. 2, pp. 23 – 30.

[16] A. J. M. Pemen *et al*, "On-line partial discharge monitoring of HV components", *Eleventh International Symposium on High Voltage Engineering (IEE Conf. Publ. No. 467)*, 1999, vol. 5, pp. 136 - 139.

[17] P. J. Moore, I. E. Portugues and I. A. Glover , "Pollution of the radio spectrum from the generation of impulsive noise by high-voltage equipment", *IEE Conference on Getting the most out of the radio spectrum,* London, October 2002, IEE Publication 02/112, pp 37/1 -37/5.

XIII. BIOGRAPHY

Philip Moore (M' and SM'1996) was born in Liverpool, England in 1960. He received his BEng in Electrical Engineering from Imperial College London in 1984 and his PhD in Power System Protection from City University London in 1989. From 1984 to 1987, he was a Development Engineer at Alstom Protection and Control, formerly GEC Measurements. From 1987 to 1991 he was a lecturer in Electrical Engineering at City University. He joined the University of Bath in 1991 where he is presently a Senior Lecturer. Dr Moore's research interests include radio frequency emissions from power system plant, harmonics, numeric protection, high voltage discharges, power system simulation and fault location. Dr Moore is a Chartered Engineer in the UK.

Iliana Portugués was born in Madrid, Spain in 1979. She graduated with a MEng degree in Electronic and Communication Engineering from the University of Bath in 2001. She was awarded a University Departmental prize for her work on harmonics measurement. She is currently employed at the University of Bath as a Research Officer in the Department of Electronic and Electrical Engineering, investigating the characteristic radio frequency emissions from defective substation insulation.

Ian Glover trained, between 1975 and 1981, as a power engineer with the Yorkshire Electricity Board (UK) graduating from the University of Bradford (UK) in 1981 with a BEng degree in Electrical and Electronic Engineering. Between 1981 and 1984 he worked as a research student at the University of Bradford. Between 1984 and 1999 he was employed at the University of Bradford, first as a lecturer in Electronic and Electrical Engineering and subsequently as a senior lecturer. In 1987 he was awarded a PhD for a thesis on microwave cross-polarisation by the University of Bradford. In 1999 he moved to the University of Bath (UK) where he is currently a senior lecturer in telecommunications. Ian Glover is, with Peter Grant, the author of Digital Communications published by Prentice-Hall. His principal research interests are in the areas of radio science and radio systems, including channel modeling, channel measurements and the impulsive noise environment.